Materials Advances

Accepted Manuscript

This article can be cited before page numbers have been issued, to do this please use: S. R. Patel, I. Patel, M. S. Dave, N. J. Faldu and T. Sharma, *Mater. Adv.*, 2026, DOI: 10.1039/D6MA00006A.

ROYAL SOCIETY OF CHEMISTRY

rsc.li/materials-advances

DOI: 10.1039/D6MA00006A

Covalent triazine-capped Fe_3O_4 nano composite for efficient dye remediation: structural insights, adsorption mechanism, and recyclability

Shital R. Patel [1,a], Isha R. Patel[2], Mehul S. Dave[3], Nilkanth J. Faldu[4], Tejas C. Sharma[5]

[1,a] *Department of Chemical sciences, N. V. Patel College of Pure & Applied Science, Charutar Vidya Mandal University, Gujarat- 388120, India.*

[2]*Department of Organic Chemistry, Institute of science & Technology for Advanced Studies & Research, The Charutar Vidya Mandal University, Vallabh vidyanagar, Anand, Gujarat 388120, India.*

[3]*Department of physics, N. V. Patel College of Pure & Applied Science, Charutar Vidya Mandal University, Gujarat- 388120, India.*

[4]*Department of biological sciences, N. V. Patel College of Pure & Applied Science, Charutar Vidya Mandal University, Gujarat- 388120, India.*

[5]*Department of mathematical sciences, N. V. Patel College of Pure & Applied Science, Charutar Vidya Mandal University, Gujarat- 388120, India.*

Corresponding authors' email: [a]email-shital28993@gmail.com

Abstract

The synthesis of covalent triazine framework (CTFs) conventionally requires prolonged reaction time, particularly when prepared through nucleophilic substitution between 2,4,6-trichloro-1,3,5-triazine (TCT) and amino acid based functional monomers. In this study, a Fe_3O_4-adn-(1,3,5-triazine-2,4,6-triyl)triproline nanocomposite was successfully synthesised and characterised by FT-IR, DSC, TGA, XRD, SEM and VSM analyses. The developed material demonstrates excellent adsorption proportion for the removal of hazardous industrial dyes including Reactive Red-195 (RR-195), Reactive Blue-222 (RB-222), and Reactive Black-5 (RB-5). Batch adsorption studies at 10% dye concentrations under alkaline conditions revealed high removal efficiencies of 95.8% (RR-195), 95.0% (RB-222), and 94.6% (RB-5) from real industrial effluents. Kinetic modelling indicate that the adsorption follows a pseudo-second-order mechanism, while isotherm analysis confirmed suitability of Langmuir adsorption model, suggesting mono layer adsorption. Reusability testing further showed that adsorption retained over 65% removal efficiency after ten successive cycles, establishing in potential as a sustainable, cost effective and recyclable material for waste water treatment and dye remediation applications.

Key words: nanocomposite, covalent triazine framework, industrial effluents, adsorption kinetics, Langmuir isotherm

View Article Online
DOI: 10.1039/D6MA00006A

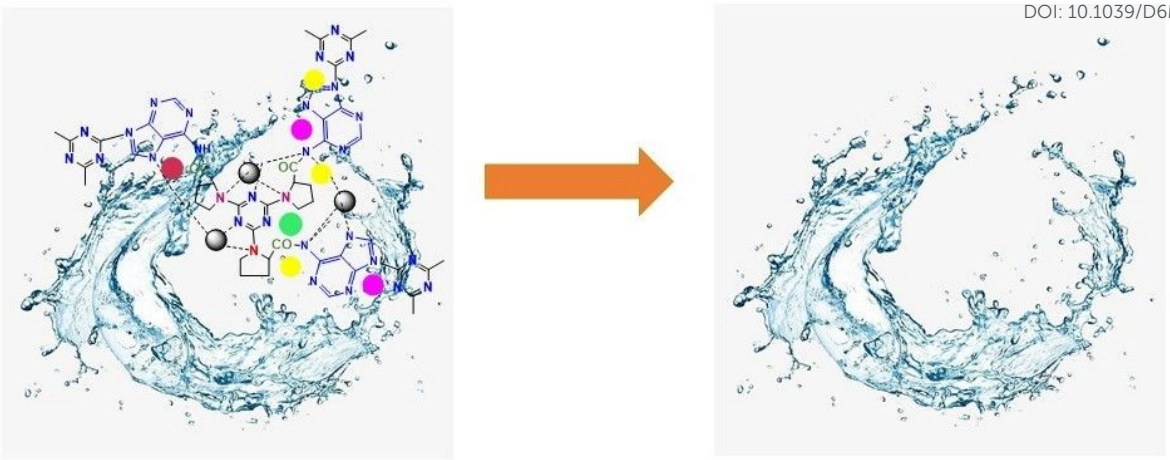

Scheme 1 A scheme showing Fe_3O_4-adn-(1,3,5-triazine-2,4,6-triyl)triproline nanocomposite and use for removing industrial organic dyes.

1. Introduction

Industrial wastewater establishes a substantial source of aquatic contamination, threatening both ecological equilibrium and human health. Among miscellaneous industrial effluents, printing and dyeing wastewater from textile industry is predominantly stressful due to its discriminating chemical oxygen demand (COD), high concentration of hazardous organic compounds, and pronounced colors [1-6]. The textile dyeing business produces wastewater weighed down with synthetic colors, hence escalating environmental contamination. Water that has been contaminated with dye can irrigate the eyes and skin when breathed in or touched. It is also linked to allergy reaction like conjunctivitis, contact dermatitis, asthma and rhinitis. Research has shown that azo dyes can interfere with ovulation and sperm production, whereas reactive dyes may attach to human serum albumin, causing the body to make immunoglobulin E and release histamine. Azo dyes have been linked to cancer in organs like the liver, bladder, and spleen, as well as chromosomal problems and mammalian cells [7-12]. It is very important for industries that use dyes to cleanse wastewater that contains dyes properly before releasing it into bodies of water. This is because dye-contaminated wastewater poses serious threats to health and the environment.

A diverse array of physiological and biological techniques has been employed to assuage wastewater contamination, encircling membrane filtration, flocculation, co-precipitation, photodegradation, and biological treatment. Among these stratagems, adsorption onto porous materials has publicized to be one of the most successful methods owing to its high efficiency, low operation cost, simplicity, and environmental compatibility. Recent years have seen an increase in environmental alertness and governing focus, leading to discriminating interest in

View Article Online
DOI: 10.1039/D0MA00006A

the development of sustainable materials that provide an eco-friendly and economical reasonable solution for industrial wastewater treatment and abolition of toxic organic pollutants [13-18].

The employment of magnetic particle technology for environmental redress has harvested momentous research interest in recent year. Magnetic adsorbents provide an exceptional benefit, as they can be fluently extracted from aqueous solutions using an external field, smoothing effective recovery and reutilization. Miscellaneous magnetic adsorbent-including magnetic nanoparticles, organic group modified and chitosan, along with magnetic Fe_3O_4 particles-have been engineered and thoroughly considered for the abstraction of dyes from wastewater. The manufacture of these magnetic materials is recurrently elaborate, with frequent preliminary processes and surface changes, moreover, several of these materials have low surface areas, leading to restricted adsorption capabilities, hence limiting their practical utility in extensive wastewater treatment systems [19-26].

2,4,6-Trichloro-1,3,5-Triazine (TCT), also referred to as cyanuric chloride, is a significant heterocyclic chemical that structurally resembles aromatic benzene, including altering carbon and nitrogen atoms. The electron-deficient triazine ring core has robust electron accepting properties, facilitating diverse interaction with various contaminants. The features of TCT render are a persuasive predecessor for the amalgamation of functional polymers and hybrid materials with regenerable compatibilities, appropriate for applications together with photocatalysis, adsorption, and environmental remediation [27].

In this respect, surface functionalisation obliges as an admirable process to improve fussiness and customise surface properties for particular applications. An effective method to functionalize L-proline and adenine while preservative their intrinsic structural integrity is the assimilation of organic functional groups into the surface. The amendment of the L-proline and adenine with reactive functionalities that permit the ensuing grafting of organic moieties offers an approach to the construction of hybrid materials. These functionalised systems validate improved kinship for dyes with both hydrophobic and hydrophilic groups, allowing the effective adsorptive removal of a prevalent array of contaminated for aquatic environments [28-30].

To sum up, we have successfully developed a covalently functionalised triazine-capped Fe_3O_4 nanocomposite that functions as an extremely effective magnetically recoverable adsorbent for removing reactive dyes from wastewater solutions. Numerous active sites that facilitate strong

View Article Online
DOI: 10.1039/D6MA00006A

interaction, and π-π interactions are introduced when nitrogen-rich triazine groups are incorporated onto the surface Fe_3O_4 [31-34]. The high adsorption capacity, rapid adsorption kinetics, and remarkable magnetic separability of this resultant nanocomposite enable effective adsorbent recovery and reuse without appreciable performance degradation over multiple cycles [35-37]. The current material advantages are due to direct covalent surface modification, which increases the availability of active sites and improves adsorption efficiency when compared to previously reported magnetic triazine-based systems [38]. According to result, magnetic nanocomposites functionalised with triazine provide a promising basis for developing recyclable adsorbents for wastewater treatment [39].

This study seeks to create hybrid structure of L-proline, adenine, magnetite nanoparticles with multifunctional capabilities by strategic chemical design. This method tangled the careful selection of organic components, emphasizing molecules having functional groups that may easily abbreviate with carboxylate function on L-proline surface and amino group on adenine. The adsorption efficacy of these materials was asses using Reactive Red-195, Reactive Blue-222, Reactive Black-5 dyes as representative industrial contaminants. Essential adsorption constraints were refined, and the equilibrium data were evaluated utilising Langmuir and Freundlich isotherm models, while the kinetics of the physiological adsorption process were methodically scrutinized.

2. Experimental section

2.1. Materials and methods

Cyanuric chloride (s-triazine, sigma-aldrich), L-proline (Loba Chemie), Adenine (Loba Chemie), Potassium carbonate (Loba Chemie), Fe_3O_4 nanoparticles with average particle size around 50-100 nm (sigma-aldrich) were used without further purification. We also got the industrial effluent from Meghmani dyes and intermediates Ltd. In Ahmedabad, Gujarat. It had a mix of three dyes: Reactive Red (RR-195), Reactive Blue 222 (RB-222) and Reactive Black-5 (RB-5). The chemical structure and characteristics of the dyes are shown in Fig. 1. All testing methods were conducted utilizing ultrapure double-distilled water to guarantee the elimination of contaminants.

View Article Online
DOI: 10.1039/D6MA00006A

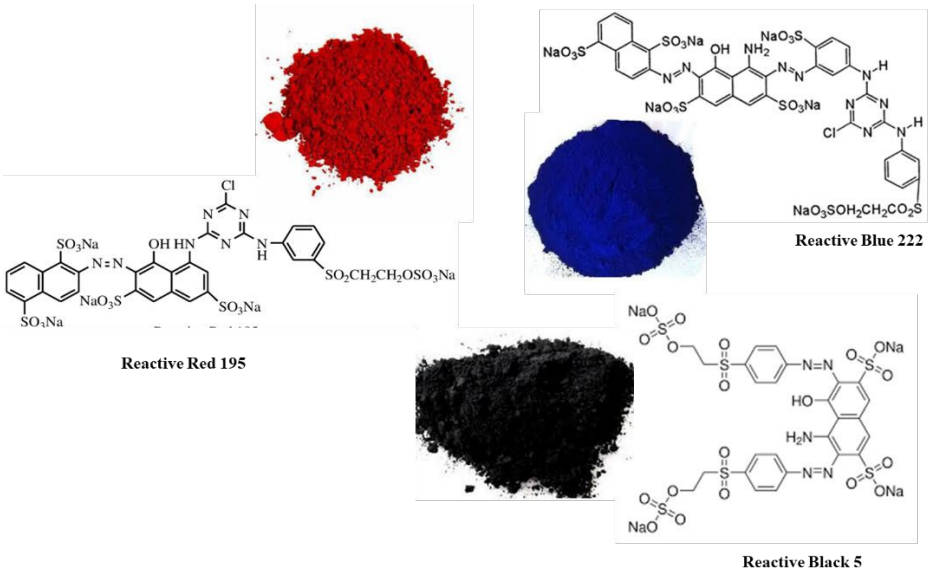

Fig.1 Characteristics of Reactive Red 195 (RR-195), Reactive Blue 222 (RB-222) and Reactive Black 5 (RB-5) dyes

2.2. Instrument and characterization

The synthesized Fe_3O_4-adn-(1,3,5-triazine-2,4,6-triyl)triproline nanocomposite was characterized to confirm its chemical structure and thermal stability. The characterization of the synthesized material was carried out using various analytical techniques, including Fourier Transform Infrared (FTIR) spectroscopy (Perkin Elmer, USA), X-ray diffraction (XRD) analysis (Bruker D8 Advance, Cu target X-ray tube, X-ray power: 2 kW, Detector: LYNXEYE XE-T, scanning range: 2° to 136°), thermogravimetric analysis (TGA) (Perkin Elmer-4000, USA), and Differential scanning calorimetry (DSC) (Perkin Elmer-800, USA). N_2 adsorption-desorption isotherm was obtained using micrometrics 3Flex analyser and smart Vac Degasser to get the surface area and pore volumes. Additionally, a UV-Vis spectrophotometer (UV/Vis 160A, Shimadzu, Japan) was used for spectroscopic analysis.

2.3 Dye adsorption studies

The adsorption experiments were conducted under controlled conditions to ensure reproducibility and accurate evaluation of adsorption performance. Batch adsorption studies were carried out 25 ± 2 ºC with continuous agitation at 150 rpm using an orbital shaker in order to maintain uniform dispersion of adsorbent and enhance mass transfer between the dye molecules and adsorption sites. The equilibrium time was set at 60 minutes based on preliminary kinetic experiments that demonstrated that adsorption equilibrium was reached within this time frame. A 10% dye concentration was selected to mimic relatively high dye

View Article Online
DOI: 10.1039/D6MA00006A

loading conditions frequently found in industrial textile effluents in order to evaluate the adsorption capacity and efficacy of the triazine-capped Fe_3O_4 nanocomposite under realistic wastewater scenarios. The adsorption performance of the Fe_3O_4-adn-(1,3,5-triazine-2,4,6-triyl)triproline nanocomposite toward Reactive Red 195(RR-195), Reactive Blue 222 (RB-222) and Reactive Black-5 (RB-5) was evaluated using batch experiments.

The adsorption kinetic experiments were carried out in 50 mL of dye effluent solution at room temperature. The synthesized material was used as an adsorbent dosage about 25 mg and added to the Reactive Red (RR-195) dye solutions with concentration 300 mg/L. The effect of solution pH, treatment time, effect of adsorbent dosage and initial dye concentration were systematically evaluated in separate experiments. After equilibrium, the solutions were analysed. The adsorption capacity and % removal was calculated using following equations.

$$q_e = (C_0 - C_e)V / m \quad \ldots\ldots\ldots\ldots\ldots \quad (1)$$

where C_0 and C_e (mg/L) are the initial and equilibrium concentrations of dyes, respectively; V (L) is the volume of the solution; and m (g) is the synthesized materials.

$$\mathrm{R}\,(\%) = (C_0 - C / C_0)\, X\, 100 \ldots\ldots\ldots\ldots\ldots\ldots (2)$$

where C_0 is the initial concentration of dye, C is the equilibrium concentration, V is the volume of the solution, m is the mass of adsorbate.

3. Results and discussion

3.1. Synthesis of (4,6-dichloro-1,3,5-triazin-2-yl)proline

A mixture of cyanuric chloride (18.44 g, 0.1 mol) in acetone was agitated with an aqueous sodium bicarbonate solution (8.40 g in 100 mL of distilled water) at 0-5 °C for 2 hours. A solution of L-proline (11.51 g, 0.1 mol) was added dropwise to the cooled reaction mixture while maintaining continuous stirring. The reaction was sustained at a constant temperature for a further 3 hours to guarantee full substitution. The resultant solid precipitate was filtered, meticulously rinsed with distilled water, and dried. The crude product was subsequently recrystallized from ethanol to provide the purified L-proline-substituted cyanuric chloride derivative.

2.2. Synthesis of (1,3,5-triazine-2,4,6-triyl)triproline

A solution of (4,6-dichloro-1,3,5-triazin-2-yl)L-proline (26.03 g, 0.1 mol) in 40 mL of acetone was incrementally added to a stirred mixture of sodium hydroxide (16 g, 0.4 mol) and L-proline

View Article Online
DOI: 10.1039/D6MA00006A

(23.03 g, 0.2 mol) at ambient temperature. The reaction mixture was agitated constantly for 3 hours, then refluxed at 80 °C for a further 3 hours to pledge complete condensation. Upon completion of the reaction, the resultant precipitate was collected via filtration, meticulously washed with distilled water, and dried. The crude product underwent purification via recrystallization from acetone to provide the required chemical. The Fujiwara test revealed the lack of unreacted dichloro-s-triazine, confirming effective substitution and the purity of the final product.

2.3. Synthesis of Fe_3O_4-adn-(1,3,5-triazine-2,4,6-triyl)triproline nanocomposite

To synthesize triazine-modified magnetic polymeric networks, activated Fe_3O_4 (0.50 g) was initially disseminated in N,N-dimethylformamide (DMF, 50 mL) and sonicated for 1 hour to get a homogenous suspension. Subsequently, 37.84 g of (1,3,5-triazine-2,4,6-triyl)triproline, stirred mixture of sodium hydroxide and adenine (13.51 g, 0.1 mol) were incorporated into the mixture, and the reaction was refluxed for 48 hours with constant agitation. Upon completion, the black solid product was magnetically separated, meticulously cleaned with ethanol and deionized water, and subsequently dried at ambient temperature. Fig. 2. presents a schematic illustration of the preparation of Fe_3O_4-adn-(1,3,5-triazine-2,4,6-triyl)triproline nanocomposite.

View Article Online
DOI: 10.1039/D6MA00006A

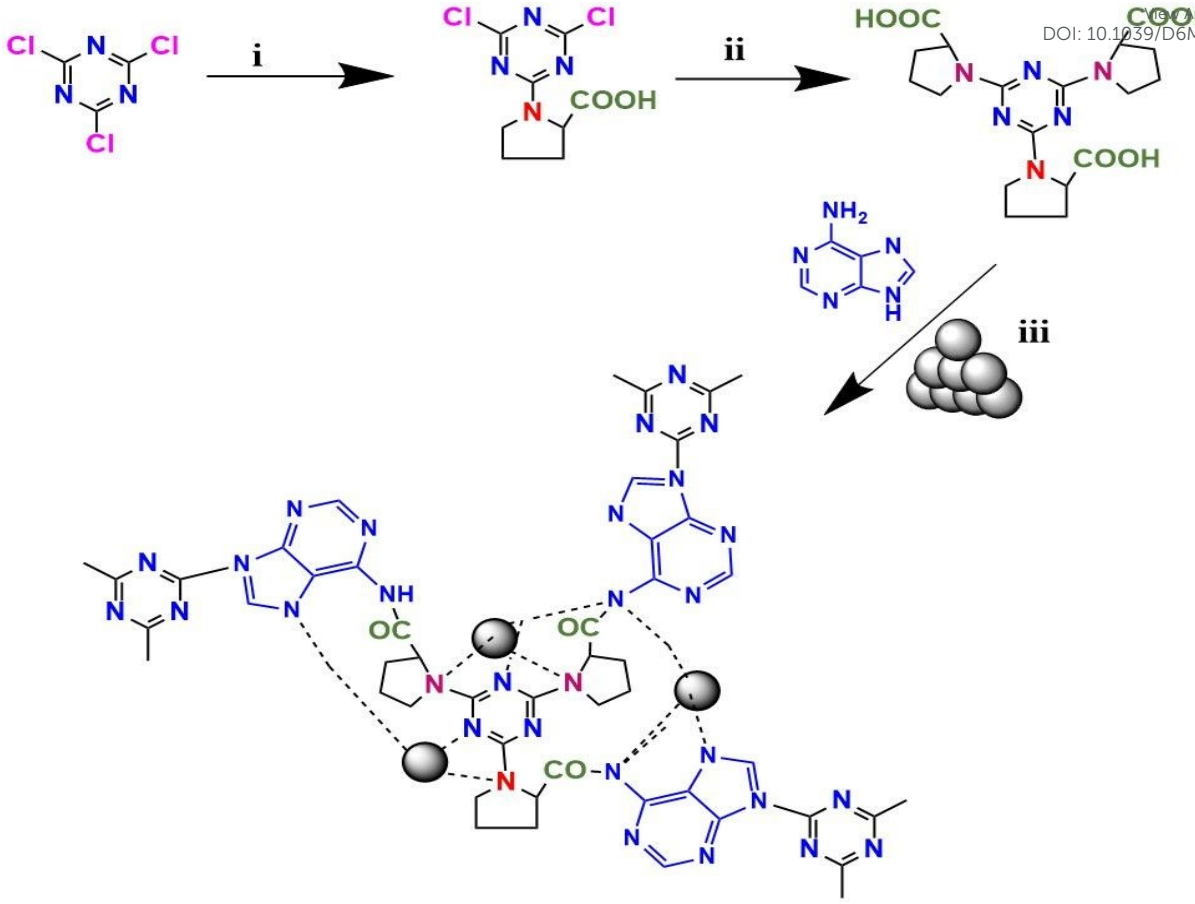

Scheme-1 Synthetic route of Triazine-Modified Magnetic Polymeric Networks
Reagent and conditions: (i) $NaHCO_3$, Acetone, 0–5°C, 2 h
(ii) NaOH, acetone, RT, 3 h, further stir at 80°C, 3 h
(iii) Fe_3O_4, Adenine, DMF, 170–190 °C, 8 h

Fig. 2. Plausible reaction scheme and structure of Fe_3O_4-adn-(1,3,5-triazine-2,4,6-triyl)triproline nanocomposite

3. Result and discussion

3.1. Fourier transform infrared (FTIR)

3.1.1. FTIR of (4,6-dichloro-1,3,5-triazin-2-yl)proline

The FTIR (Fig.3A) Spectra of (4,6-dichloro-1,3,5-triazin-2-yl)proline exhibited a wide band at 3157 -3070 cm^{-1} indicative of O-H/N-H stretching vibrations. A prominent peak at 1674 cm^{-1} was attributed to the C=O stretching pf proline unit, whilst band between 1624 and 1574 cm^{-1} were ascribed to -CH_2 and C-N vibrations, whereas the range of 845-700 cm^{-1} exhibited distinctive C-Cl stretching, corroborating the synthesis of the intended triazine-proline derivative.

3.1.2. FTIR of (1,3,5-triazine-2,4,6-triyl)triproline

View Article Online
DOI: 10.1039/D6MA00006A

The FTIR (Fig.3B) spectra of (1,3,5-triazine-2,4,6-triyl)triproline shown large adsorptions at 3080-2924 cm^{-1}, attributed to O-H and N-H stretching vibrations. Prominent bands at 1751 and 1710 cm^{-1} are indicative of C=O stretching, whereas peaks in the range of 1593-1508 cm^{-1} signify attributed to C-N and CH_2 vibrations, whereas bands at 833-542 cm^{-1} validated triazine ring deformation and skeletal modes. These characteristics together simplify the institution of the triazine-proline network.

3.1.3. FTIR of Fe_3O_4-adn-(1,3,5-triazzine-2,4,6-triyl)triproline nanocomposite

The FTIR (Fig.3C) spectrum of Fe_3O_4-adn-(1,3,5-triazine-2,4,6-triyl)triproline nanocomposite has a wide band at 3209-3053 cm^{-1}, ascribed to the overlapping O-H/N-H stretching of adenine and proline, alongside aliphatic C-H bands at 2885 and 2833 cm^{-1}. Intense adsorption at 1776-1714 cm^{-1} and 1061-1051 cm^{-1} correspond to C-N/C=C skeleton and C-N/C-O stretching vibrations, respectively. The peaks at 842-763 cm^{-1} result from vibrations of the triazine/adenine ring. The distinctive Fe-O stretching bands 540, 447 and 419 cm^{-1} validate the presence of the magnetite core and effective organic capping.

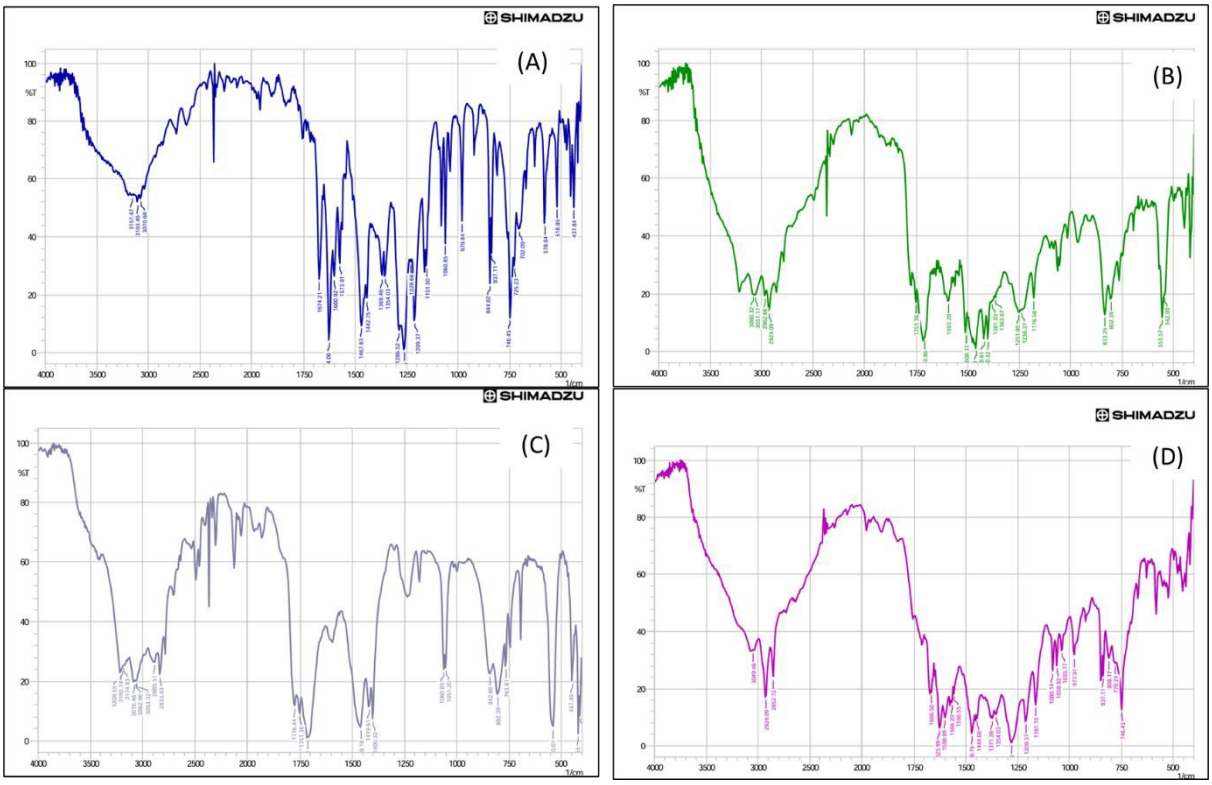

Fig. 3. FTIR spectra of (4,6-dichloro-1,3,5-triazin-2-yl)proline (A), (1,3,5-triazine-2,4,6-triyl)triproline (B) and Fe_3O_4-adn-(1,3,5-triazine-2,4,6-triyl)triproline nanocomposite(C) FTIR spectrum of regenerated Fe_3O_4-adn-(1,3,5-triazine-2,4,6-triyl)triproline nanocomposite after adsorption-desorption cycles (D)

View Article Online
DOI: 10.1039/D6MA00006A

3.1.4. FTIR of regenerated Fe_3O_4-adn-(1,3,5-triazzine-2,4,6-triyl)triproline nanocomposite

FTIR spectroscopy (Fig.3D) was used to assess the structural stability of Fe_3O_4-adn-(1,3,5-triazine-2,4,6-triyl)triproline nanocomposite following adsorption-desorption cycles. The spectrum demonstrates that the regenerated material maintained the distinctive vibrational bands seen in the new adsorbent. Aromatic C-H stretching is represented by the bands at 3094 cm^{-1}, whereas aliphatic C-H vibrations are represented by the bands at 2924 and 2852 cm^{-1}.the triazine ring C=N stretching is responsible for the prominent peak at 1665 cm^{-1}, while aromatic ring vibrations are represented by the bands at 1598-1556 cm^{-1}. While bands at 1209-1035 cm^{-1} show C-N/C-O vibrations, peaks at 1444-1354 cm^{-1} are the result of C-N stretching. The preservation of the Fe_3O_4 core is confirmed by the Fe-O stretching band in low-frequency region. The significant shift in peak locations show that the chemical framework is unaltered following recycling.

3.2. Different scanning calorimetry (DSC)

3.2.1. DSC of Fe_3O_4-adn-(1,3,5-triazine-2,4,6-triyl)triproline nanocomposite

The DSC thermogram (Fig.4A) Fe_3O_4-adn-(1,3,5-triazine-2,4,6-triyl)triproline nanocomposite displays several temperature changes, indicating the intricate structure of the hybrid nanocomposite. The slight endothermic variation noted below 120 ˚C is attributed to the release of absorbed or loosely bound moisture. Distinct glass transition events observed at 189-196 ˚C and 270-282 ˚C are ascribed to the segmental relaxation of adenine and triazine proline moieties, respectively, within polymeric shell. The extensive exothermic shift over 300 ˚C, succeeded by a significant thermal event at 493-506 ˚C, signifies ongoing structural reorganization, crosslinking, and subsequent breakdown of the organic matrix. The continuity of transition at high temperature validates the significant thermal stability and robust interfacial interaction between the Fe_3O_4 core and the organic triazine-adenine-proline framework.

3.1.2. DSC of dye absorbed Fe_3O_4-adn-(1,3,5-triazine-2,4,6-triyl)triproline nanocomposite

The DSC thermogram (Fig.4B) dye-adsorbed Fe_3O_4-adn-(1,3,5-triazine-2,4,6-triyl)triproline nanocomposite exhibits remarkable multi step thermal changes, signifying structural alteration following dye absorption. The earliest endothermic phenomenon occurring below 120 ˚C relates to desorption of physically absorbed moisture or solvent remnants. Three distinct glass transition areas are identified at 160-162 ˚C, 184-189 ˚C, and 265-287 ˚C, with corresponding C_p values of 0.234, 0.610, and 0.378 J g^{-1} K^{-1}. The lower-temperature transitions are ascribed

View Article Online
DOI: 10.1039/D5MA00006A

to localized molecular relaxations within the adenine and triazine-proline domains, whereas the higher temperature T_g indicates constrained segmental motion resulting from robust interfacial interaction among Fe_3O_4 core, organic matrix, and adsorbed dye molecules. The lack of a significant degradation exotherm upto 400 ˚C suggests that the hybrid preserves its thermal integrity following dye absorption. The DSC profile indicates that the dye absorption improves molecular packing and thermal rigidity in Fe_3O_4-adn-(1,3,5-triazine-2,4,6-triyl)triproline nanocomposite network.

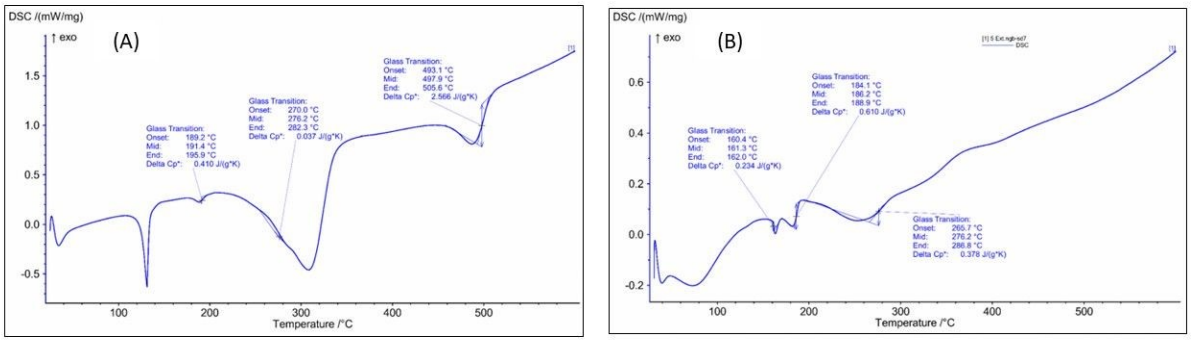

Fig. 4. DSC of Fe_3O_4-adn-(1,3,5-triazine-2,4,6-triyl)triproline nanocomposite (A) and RR-195 dye adsorbed Fe_3O_4-adn-(1,3,5-triazine-2,4,6-triyl)triproline nanocomposite (B)

3.3. Thermogravimetric analysis (TGA)

3.3.1. TGA of Fe_3O_4-adn-(1,3,5-triazine-2,4,6-triyl)triproline nanocomposite

The TGA curve (Fig.5A) of Fe_3O_4-adn-(1,3,5-triazine-2,4,6-triyl)triproline nanocomposite displays two significant stages of weight reduction. The initial substantial loss of around 70.5% within the temperature range of 50-320 ˚C is attributed to the elimination of physically absorbed water and the degradation of surface-attached chemical groups, including adenine, triazine, and proline moieties. The second stage, accounting for roughly 27.4% between 350-500 ˚C, is ascribed to the breakdown of the residual organic matrix covalently bonded to the Fe_3O_4 surface. Above 500 ˚C, the mass remains relatively unchanged, signifying the establishment of thermally stable Fe_3O_4 residue. The results validate effective capping of Fe_3O_4 nanoparticles with the organic triazine-adenine-proline framework, resulting in improved thermal stability.

3.3.2. TGA of dye adsorbed Fe_3O_4-adn-(1,3,5-triazine-2,4,6-triyl)triproline nanocomposite

The TGA (Fig.5B) profile of dye-adsorbed Fe_3O_4-adn-(1,3,5-triazine-2,4,6-triyl)triproline nanocomposite reveals three discrete stages of weight loss. The preliminary 3.8% reduction below 140 ˚C is ascribed to the elimination of physically adsorbed water and moisture. The

View Article Online
DOI: 10.1039/D6MA00006A

principal decomposition phase of approximately 39.5% occurring between 200-350 ˚C pertains to the thermal degradation of the organic coating, encompassing adenine, triazine, proline linkages, and the adsorbed dye molecules. Additional 8.2% loss between 400-500 ˚C results from the degradation of tightly bonded residual organic constituents and dye fragments. Above 550 ˚C, the curves stabilize, signifying the existence of thermally stable Fe_3O_4 residue. This thermal pattern validates effective dye adsorption and robust stability of the organic- inorganic hybrid.

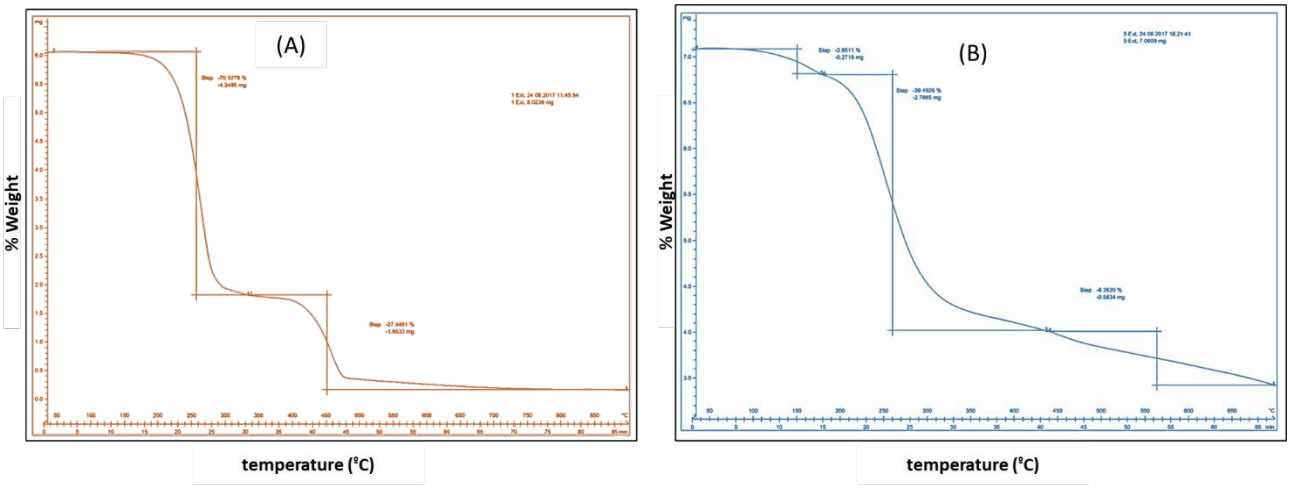

Fig. 5. TGA curves of Fe_3O_4-adn-(1,3,5-triazine-2,4,6-triyl)triproline nanocomposite (A) and RR-195 dye adsorbed Fe_3O_4-adn-(1,3,5-triazine-2,4,6-triyl)triproline nanocomposite (B)

3.4. XRD of Fe_3O_4-adn-(1,3,5-triazine-2,4,6-triyl)triproline nanocomposite

The XRD (Fig.6) pattern of Fe_3O_4-adn-(1,3,5-triazine-2,4,6-triyl)triproline nanocomposite exhibits distinct diffraction peats at 2θ ≈ 30.2, 35.5, 43.2, 53.6, 57.1, and 62.7, which correspond to the (220), (311), (400), (422), (551), and (440) planes of cubic inverse spinal Fe_3O_4 (JCPDS No. 19-0629). The lack of contaminant phases verifies the phase purity of magnetite. A diffuse broad background in the 15-30˚ range is ascribed to the amorphous organic capping layer. The persistence of Fe_3O_4 diffraction peaks post-functionalization signifies effective surface capping without modification of the crystalline structure, validating the creation of Fe_3O_4 based organic-inorganic composite.

View Article Online
DOI: 10.1039/D6MA00006A

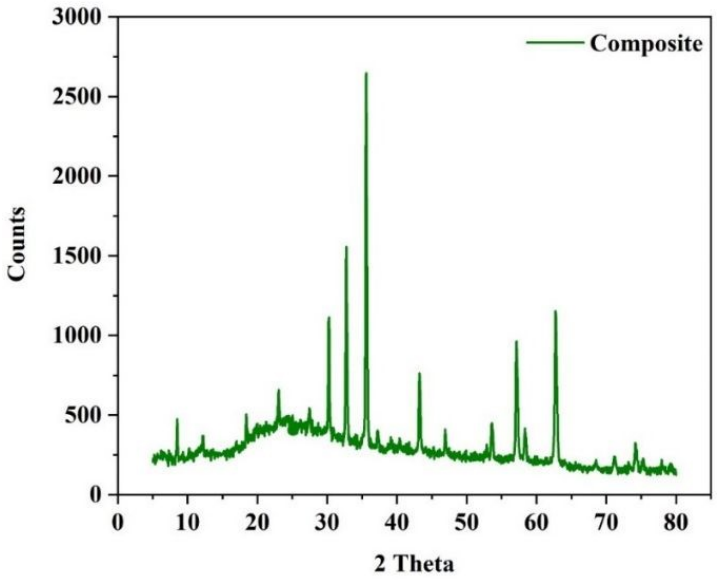

Fig. 6. XRD Patterns of Fe_3O_4-adn-(1,3,5-triazine-2,4,6-triyl)triproline nanocomposite

3.5. Vibrating sample magnetometer (VSM)

The VSM hysteresis loop (Fig.7) of Fe_3O_4-adn-(1,3,5-triazine-2,4,6-triyl)triproline nanocomposite displays an S-shaped curve with little coercivity (Hc<50 Oe) and exceedingly low remanence, indicating, indicating super magnetic characteristics at ambient temperature. The saturation magnetisation (Ms ≈ 0.26 emu) is inferior to that of bare Fe_3O_4, a phenomenon ascribed to the existence of the non-magnetic triazine-triproline capping layer. nonetheless, the composite preserves adequate magnetic responsiveness, facilitating effective magnetic separation while upholding surface functionalization.

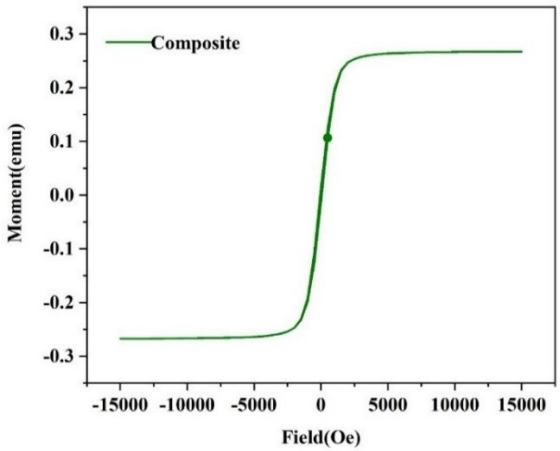

Fig. 7. Magnetic hysteresis curve of Fe_3O_4-adn-(1,3,5-triazine-2,4,6-triyl)triproline nanocomposite

View Article Online
DOI: 10.1039/D6MA00006A

3.6 Brunauer-Emmett-Teller analysis

The observed adsorption performance of the materials is highly correlated with textural properties obtained from BJH and BET analyses (Fig.8). With a well-defined mesoporous structure (~20 Aº) and a higher specific surface area (~180-220 m^2 g^{-1}), the binder-less sample offers more accessible active sites, which directly contributes to its higher adsorption capacity (q_e) in comparison to Fe_3O_4-adn-(1,3,5-triazine-2,4,6-triyl)triproline nanocomposite. Mass transfer resistance is reduced by the enhanced pore volume and homogeneous mesopore distribution, which promote effective dye molecule diffusion into the internal pore network.

From a kinetic standpoint, Fe_3O_4-adn-(1,3,5-triazine-2,4,6-triyl)triproline nanocomposite increased mesoporosity facilitates quicker adsorption rates, which are in line with the pseudo-second-order kinetic model and suggest that chemisorption involving surface functional groups is important. Furthermore, by enhancing interparticle diffusion, the existence mesopores facilities quick equilibrium attainment. Nanocomposite superior surface properties favor monolayer adsorption behaviour in terms of adsorption isotherms, as shown by a better fit to the Langmuir isotherms, indicating a homogeneous distribution of active sites. Fe_3O_4-adn-(1,3,5-triazine-2,4,6-triyl)triproline nanocomposite comparatively smaller surface area and pore volume lead to slower kinetics and decreased adsorption capacity, underscoring the crucial role of textural characteristics. Overall, the combined BJH-BET and adsorption analyses show that the binder-less material improved mesoporosity and surface area are important factors controlling its enhanced adsorption efficiency, favorable kinetics, and strong isotherm behaviour, confirming its potential as an effective adsorbent for dye removal applications.

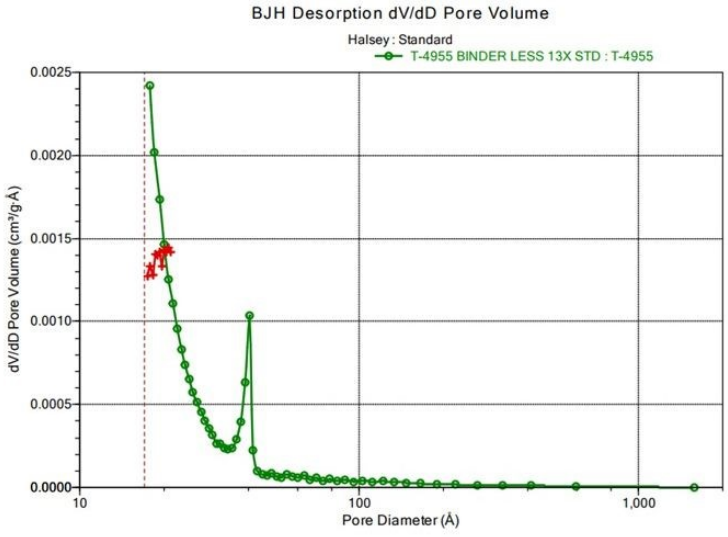

Fig. 8 BJH desorption pore size distribution (dv/dD vs. pore diameter) of the synthesized sample calculated using Hasley standard model

View Article Online
DOI: 10.1039/D6MA00006A

3.7 Optimization of dye removal performance data

Optimization is a very important part of every analytical process since it makes the approach more sensitive and accurate in different situations. By fine-tuning the settings, it helps the system work at its best while still being able to handle the intricacies and variety of real-world samples.

3.7.1. Effect of pH

Fig. 9 illustrates the impact of pH removal efficiency of the dyes RR-195, RB-222, and RB-5. Dye removal was notably elevated at alkaline condition, especially for RR-195 and RB-5, owing to the protonation of surface functional groups that intensifies electrostatic attraction with reactive dye molecules. A reduction in removal effectiveness was noted in the immediate pH range, attributable to diminished surface charge density and poorer dye-adsorbent interactions. At alkaline pH, the removal efficiency for all dyes markedly increased, attaining peak values at pH 12 (about 90% for RR-195, approximately 89% for RB-5, and approximately 88% for RB-222). The boost correlates with high tended ionisation of functional groups on the adsorbent surface, facilitating stronger interactions with dye molecules. The consistently elevated elimination of RR-195 indicates a stronger affinity for the adsorbent. Low standard deviation values (SD<1%) signify excellent experimental repeatability.

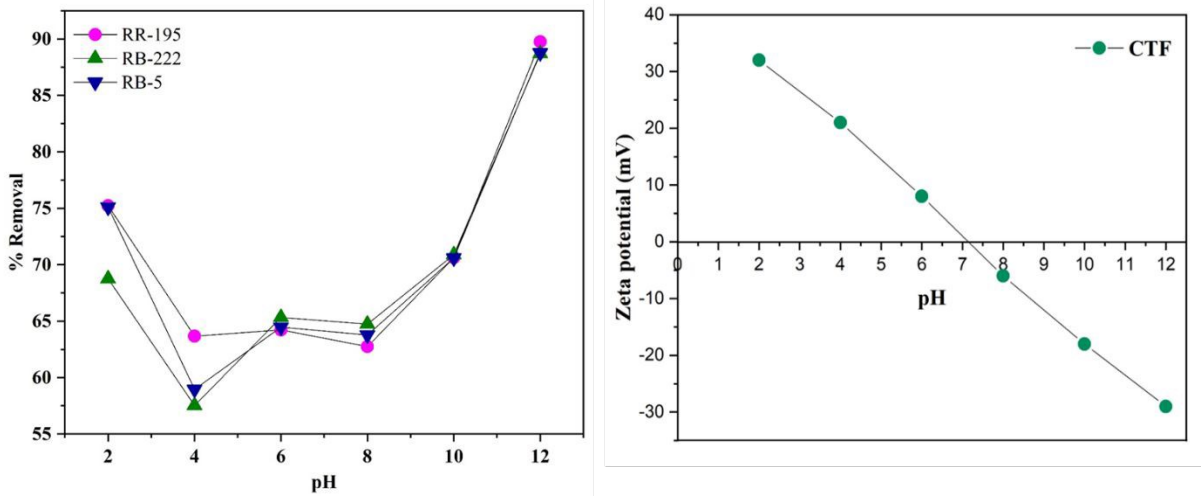

Fig. 9. Effect of pH on % removal RR-195, RB-222 and RB-5 dyes of Fe_3O_4-adn-(1,3,5-triazine-2,4,6-triyl)triproline nanocomposite (adsorbent dose=10 mg, solution volume=50 ml, solid-liquid ratio= 0.2 g L^{-1}, temperature= 298 K)

Fig. 10. Zeta potential analysis of the Fe_3O_4-adn-(1,3,5-triazine-2,4,6-triyl)triproline nanocomposite

View Article Online
DOI: 10.1039/D6MA00006A

Zeta potential measurements were assessed over a pH range of 2-12 in order to comprehend the surface charge behaviour of the synthesized triazine-functionalised Fe_3O_4 nanocomposite. Because it regulates the electrostatic interactions between the adsorption of reactive dyes. The findings show that the zeta potential gradually drops as pH rises, going from positive values in acidic environments to negative values in alkaline ones. The triazine-functionalised Fe_3O_4 nanocomposite point of zero charge (pHpzc) is found at pH 6-7. The protonation of nitrogen-containing functional groups in the triazine ring causes the adsorbent surface to become positively charged at pH values below pHpzc. This increases the electrostatic attraction between the negatively charged sulfonate groups of the reactive dyes (RR-195, RB-222 and RB-5) and positively charged adsorbent surface. A negatively charged adsorbent surface is produced when the pH rises above the pHpzc due to the protonation of surface functional groups. Adsorption may occur in this area via hydrogen bonding interactions with surface functional groups and π-π interaction between the aromatic structures of dye molecules and the triazine rings. These findings verify that the pH-dependant adsorption behaviour seen in Fig. 10 is explained by an adsorption mechanism that combines hydrogen bonding, interactions, and π-π electrostatic attraction.

3.7.2. Effect of contact time

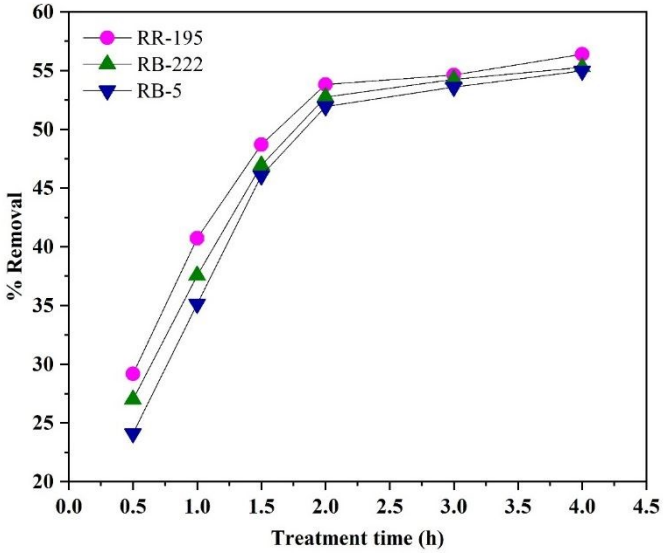

Fig. 11. Effect of treatment time on % removal RR-195, RB-222 and RB-5 dyes of Fe_3O_4-adn-(1,3,5-triazine-2,4,6-triyl)triproline nanocomposite (adsorbent dose=10 mg, solution volume=50 ml, solid-liquid ratio= 0.2 g L^{-1}, temperature= 298 K)

View Article Online
DOI: 10.1039/D5MA00006A

Fig. 11 illustrates the impact of treatment duration on the removal efficiency of RR-195, RB-222, and RB-5 dyes. Dye removal exhibits a significant increase during the initial phases of adsorption, thereafter transitioning to slow approach to equilibrium for all three dyes. In the initial 0.5 hours, removal efficiencies around 29%, 27% and 24% were attained for RR-195, RB-222 and RB-5, respectively signifying rapid occupation of accessible active sites on the absorbent surface. A significant increase in dye absorption was noted during 2 hours of contact time, with removal efficiencies of 53.8% (RR-195), 52.8% (RB-222) and 51.8% (RB-5). Subsequent to this time frame, only negligible increase in removal were seen, indicating saturation of adsorption sites and the development of adsorption-desorption equilibrium. After 4 hours, the maximum removal efficiencies were approximately 56.5% for RR-195, 55.4% for RB-222, and 54.8% for RB-5. Of the examined dyes, RR-195 consistently shown marginally superior removal effectiveness at all contact duration, likely due to enhanced electrostatic interaction and a greater affinity of its functional groups for the adsorbent active sites. The same kinetic patterns exhibit by all dyes suggest that the adsorption process is predominantly regulated by surfaced controlled interactions, characteristic by fast initial uptake succeed by diffusion limited equilibrium behaviour.

3.7.3 Effect of Adsorbent Dose on Dye Removal

Fig.12 illustrates the impact of adsorbent dosage on the removal efficiency of the dyes RR-195, RB-222, and RB-5. An elevation in adsorbent dosage from 10 to 50 mg led to a substantial improvement in dye removal, attributed to augment availability of active adsorbent sites. At minimal dosage of (10 mg), removal efficiencies were very low (about 28-33 %) whereas at 50 mg peak removal efficiencies of approximately 88-90% were attained. The fast rise in removal to 30 mg signifies efficient use of newly accessible surface sites, whereas the gradual increase beyond the threshold implies partial site saturation and diminished impetus for adsorption. RB-222 and RB-5 demonstrate marginally superiority removal at elevated doses, while RR-195 exhibited relatively enhanced efficacy at lower doses.

View Article Online
DOI: 10.1039/D6MA00006A

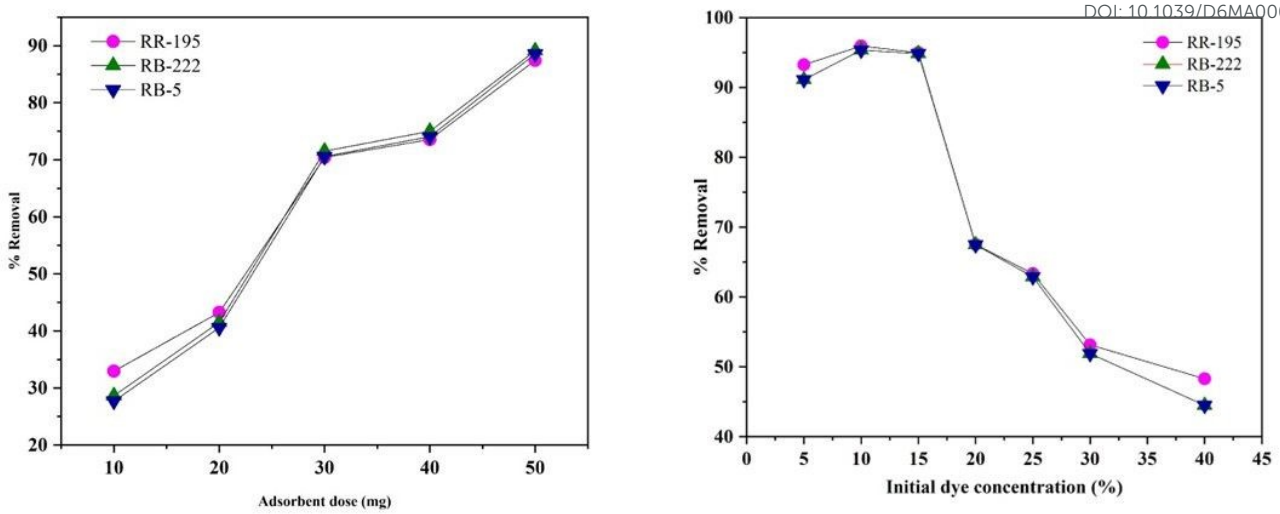

Fig. 12. Effect of adsorbent dosage on % removal RR-195, RB-222 and RB-5 dyes of Fe_3O_4-adn-(1,3,5-triazine-2,4,6-triyl)triproline nanocomposite (adsorbent dose=10-50 mg, solution volume=50 ml, solid-liquid ratio= 0.2-1.0 g L^{-1}, temperature= 298 K)

Fig. 13. Effect of initial dye concentration on % removal RR-195, RB-222 and RB-5 dyes of Fe_3O_4-adn-(1,3,5-triazine-2,4,6-triyl)triproline nanocomposite (adsorbent dose=10 mg, solution volume=50 ml, solid-liquid ratio= 0.2 g L^{-1}, temperature= 298 K)

3.7.4 Effect of initial Dye Concentration

Fig. 13 illustrates the impact of initial dye concentration on the elimination of RR-195, RB-222, and RB-5 dyes. At low concentrations (5-15%) removal efficiencies over 94% were noted for all dyes, demonstrating adequate availability of active absorption sites. Optimal elimination occurred at a 10% concentration, attaining 95.8% for RR-195, 95.0% for RB-222, and 94.6% for RB-5. A notable decline in removal efficiency was seen with an increase in dye concentration. At 40% the removal efficiencies decreased to 48.5%, 45.0%, and 44.2%, for RR-195, RB-222, and RB-5, respectively. The decrease is ascribed to the saturation of adsorption sites and high tended competition among dye molecules at elevated concentration. RR-195 consistently demonstrate marginally superior removal efficiency, indicating a greater affinity for the adsorbent surface. Minimal standard deviation values (SD<1%) indicated excellent experimental repeatability.

3.7.5 Kinetics modelling

The connection between empirical data and theoretically kinetic models was built in order to gain a deeper understanding of the adsorption mechanism. By applying pseudo-first-order (PFO) along with pseudo-second-order (PSO) models, the kinetic behaviour of RR-195

View Article Online
DOI: 10.1039/D5MA00006A

sorption onto the Fe_3O_4-adn-(1,3,5-triazine-2,4,6-triyl)triproline nanocomposite was examined (Fig. 14). Eqs. (3) and (4), correspondingly, are the linear equations for PFO and PSO, and Table 1 provides a summary of the fitting parameters.

$$\log\ (q_e - q_t) = \log\ q_e - \frac{k_1}{2.303} \cdot t \qquad \ldots (3)$$

$$\frac{t}{q_t} = \frac{1}{(k_2 \cdot q_e^2)} + \frac{1}{q_e} t \qquad \ldots (4)$$

where adsorption capabilities of the Fe_3O_4-adn-(1,3,5-triazine-2,4,6-triyl)triproline nanocomposite at equilibria and at time t (min) are denoted by q_e (mg/g) and q_t (mg/g), respectively. In the pseudo-first-order kinetic model, the rate constant is denoted as k_1 (min^{-1}), whereas in the pseudo-second-order kinetic model, the equilibrium rate constant is represented by k_2 (g mg^{-1} min^{-1}). The PSO model proposes that chemical adsorption, which is reliant on a plentiful supply of binding sites, predominates, whereas the PFO model implies diffusion as the rate-limiting step.

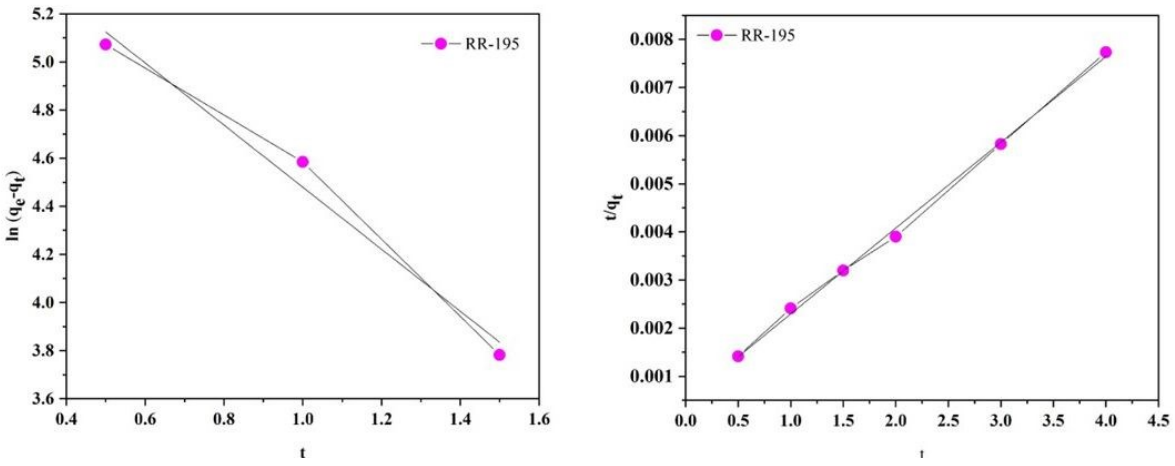

Fig. 13. Fitting curves of RR-195 dye obtained from pseudo-first-order and pseudo-second-order models

One important metric for assessing how well the model fits experimental data is the correlation coefficient (R^2). In comparison to the PFO model, the PSO model showed a higher R^2 value (0.9975), and the computed q_e values were more in line with the experimental findings. These results suggest that chemical interactions involving functional groups are primarily responsible for the adsorption of RR-195 onto the surface of Fe_3O_4-adn-(1,3,5-triazine-2,4,6-triyl)triproline nanocomposite.

View Article Online
DOI: 10.1039/D6MA00006A

Table 1 Kinetic parameters of pseudo-first-order and pseudo-second-order models for RR-195 dye onto the Fe_3O_4-adn-(1,3,5-triazine-2,4,6-triyl)triproline nanocomposite

Dye Name	Pseudo First Order			Pseudo Second Order		
	R^2	$q_{e,cal}$	k_1	R^2	$q_{e,cal}$	k_2
		mg/g	min^{-1}		mg/g	min^{-1}
RR-195	0.9613	0.7612	1.30	0.9975	555.55	0.0063

3.7.6 Adsorption Isotherm modelling

To gain deeper insight into the equilibrium adsorption of RR-195 dye onto the Fe_3O_4-adn-(1,3,5-triazine-2,4,6-triyl)triproline nanocomposite, the experiment equilibrium data obtained from the concentration-dependant adsorption experiments (Fig.15) were analysed using Langmuir and Freundlich isotherm models. The nonlinear fitting results are presented in Fig. 9, and the corresponding isotherm parameters are summarized in Table-2.

The Langmuir isotherm model, which assumes monolayer adsorption on a homogeneous surface with a finite number of energetically equivalent adsorption sites, is expressed as:

$$q_e = \frac{q_{\max} K_L C_e}{1+K_L C_e} \quad \text{.....(5)}$$

Where q_e (mgg^{-1}) is the equilibrium adsorption capacity, q_{max} ((mgg^{-1})) is the maximum monolayer adsorption capacity, K_1 (L mg^{-1}) is the Langmuir constant related to adsorption affinity, and C_e (mg L^{-1}) is the equilibrium dye concentration.

The Freundlich isotherm model, applicable to heterogeneous surfaces and multilayer adsorption, is expressed as:

$$q_e = K_F C_e^{1/n} \quad \text{.....(6)}$$

Where K_f is the Freundlich adsorption constant and 1/n represents adsorption intensity.

The Langmuir model seems to fit the adsorption of RR-195 dye better, with R^2 >0.99, which evidences that the active sites are relatively homogeneously distributed and that adsorption is primarily in monolayer (Table 2). It reflects the strong affinity of dye molecule toward Fe_3O_4 capped with Adn-(1,3,5-triazine-2,4,6-triyl)triproline.

View Article Online
DOI: 10.1039/D6MA00006A

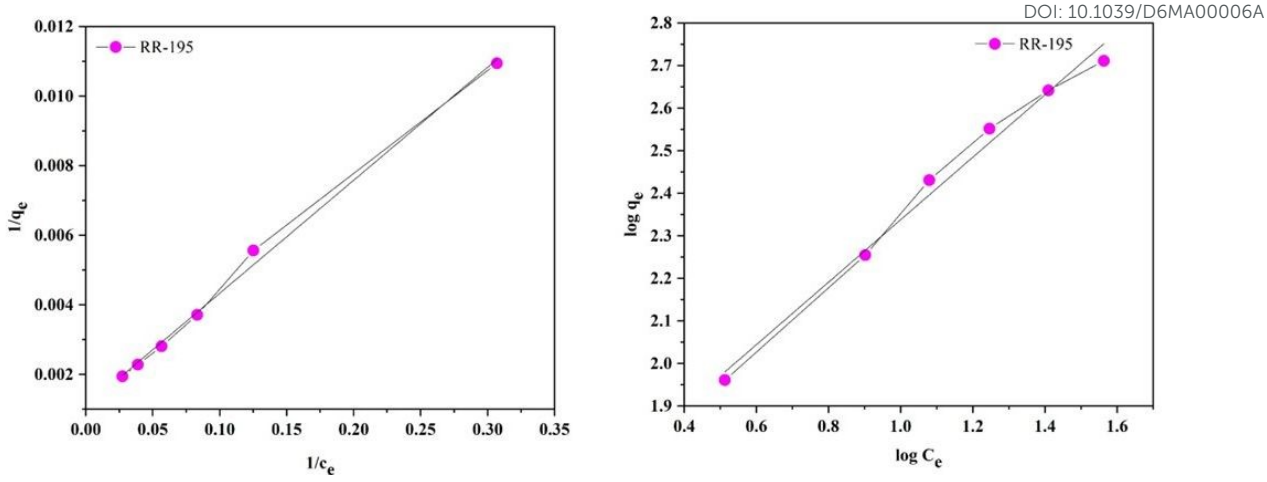

Fig. 15. Fitting curves of RR-195 dye obtained from Langmuir and Freundlich models

Table 2 Langmuir and Freundlich isotherm parameters for the adsorption of RR-195 dye onto the Fe_3O_4-adn-(1,3,5-triazine-2,4,6-triyl)triproline nanocomposite

Dye Name	Langmuir Isotherm			Freundlich Isotherm		
	R^2	q_o	b	R^2	K_f	n
RR-195	0.9956	909.09	0.0338	0.9858	0.4724	0.3623

3.7.7 Regeneration Performance

The regeneration of a dye-loaded Fe_3O_4-adn-(1,3,5-triazine-2,4,6-triyl)triproline nanocomposite was evaluated in both acidic and alkaline conditions to restore adsorption capacity. After adsorption, the nanocomposite was magnetically separated and stirred continuously for 60 minutes before being exposed to either 0.05M HCl and 0.05M NaOH. In an acidic medium, protonation of triazine nitrogen and surface hydroxyl groups decreases hydrogen-bonding and electrostatic interactions, which encourages dye desorption. Conversely, alkaline treatment deprotonates surface functional groups, creating negatively charged sites that promote electrostatic repulsion with anionic dye molecules such as reactive Red 195. The regenerated adsorbent was magnetically recovered, cleaned to neutral pH, dried at 70 ºC, and then used once more in subsequent adsorption cycles to show efficient and sustainable regeneration.

To investigate stability and practical applicability, the reusability of the Fe_3O_4-adn-(1,3,5-triazine-2,4,6-triyl)triproline nanocomposite was examined in ten consecutive adsorption

desorption cycles. From Fig. 16, it can be observed that the adsorption capacity for RR-195 decreases gradually with increasing cycle number. After ten cycles, the remaining RR-195 adsorption capacities for the Fe_3O_4-adn-(1,3,5-triazine-2,4,6-triyl)triproline nanocomposite was more than ~65% of its initial adsorption capacity, showing good structural integrity and strong retention of active functional groups. The minor loss in adsorption performance could be due to the partial blockage of active sites or incomplete desorption of residual dye molecules in the process of regeneration. Thus, according to these results, the synthesized structure possessed satisfactory reusability, confirming its potential for repeated use in the treatment of wastewater.

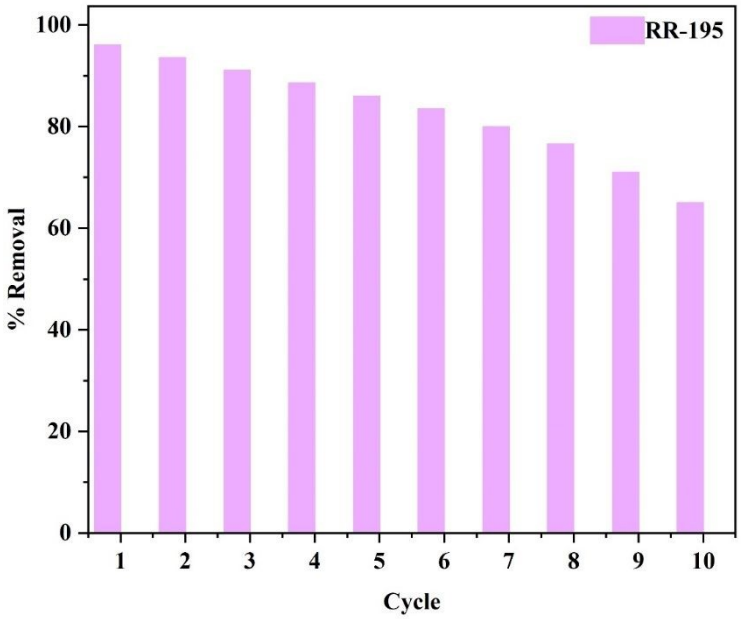

Fig. 16 Regeneration cycle

3.7.8 Dye removal mechanism

The adsorption of reactive dyes RR-195, RB-222, and RB-5 onto the triazine-modified magnetic polymeric network occurs via a synergistic, multi-interactions mechanism influenced by the surface chemistry of the adsorbent and the anionic characteristics of the dye molecules (Fig.17). In acidic to near neutral circumstances, secondary amine groups from proline units and exocyclic amine functions from adenine become protonated, resulting in positively charged polymer surface. The protonation significantly increases the electrostatic interaction between the adsorbent and the sulfonate ($-SO_2$) groups of the reactive dyes, serving as the principal driving forces for adsorption. Alongside electrostatic interactions, significant hydrogen bonding transpires between the -NH and -COOH groups within the polymeric structure and the azo (-N=N), sulfonate and heteroatom containing moieties of the dye molecules. These

View Article Online
DOI: 10.1039/D6MA00006A

interactions enhance adsorption stability and diminish dye desorption during agitation. Additionally, the π-conjugated s-triazine and adenine moieties facilitate π-π stacking the donor acceptor interactions with the frameworks of the dyes. These interactions are especially important for large planner dye molecules like RB-5 and RB-222, facilitating multilayer adsorption on the heterogeneous polymer surface. The cross-linked structure provides a high density of available functional sites, aligning with Freundlich type adsorption characteristics.

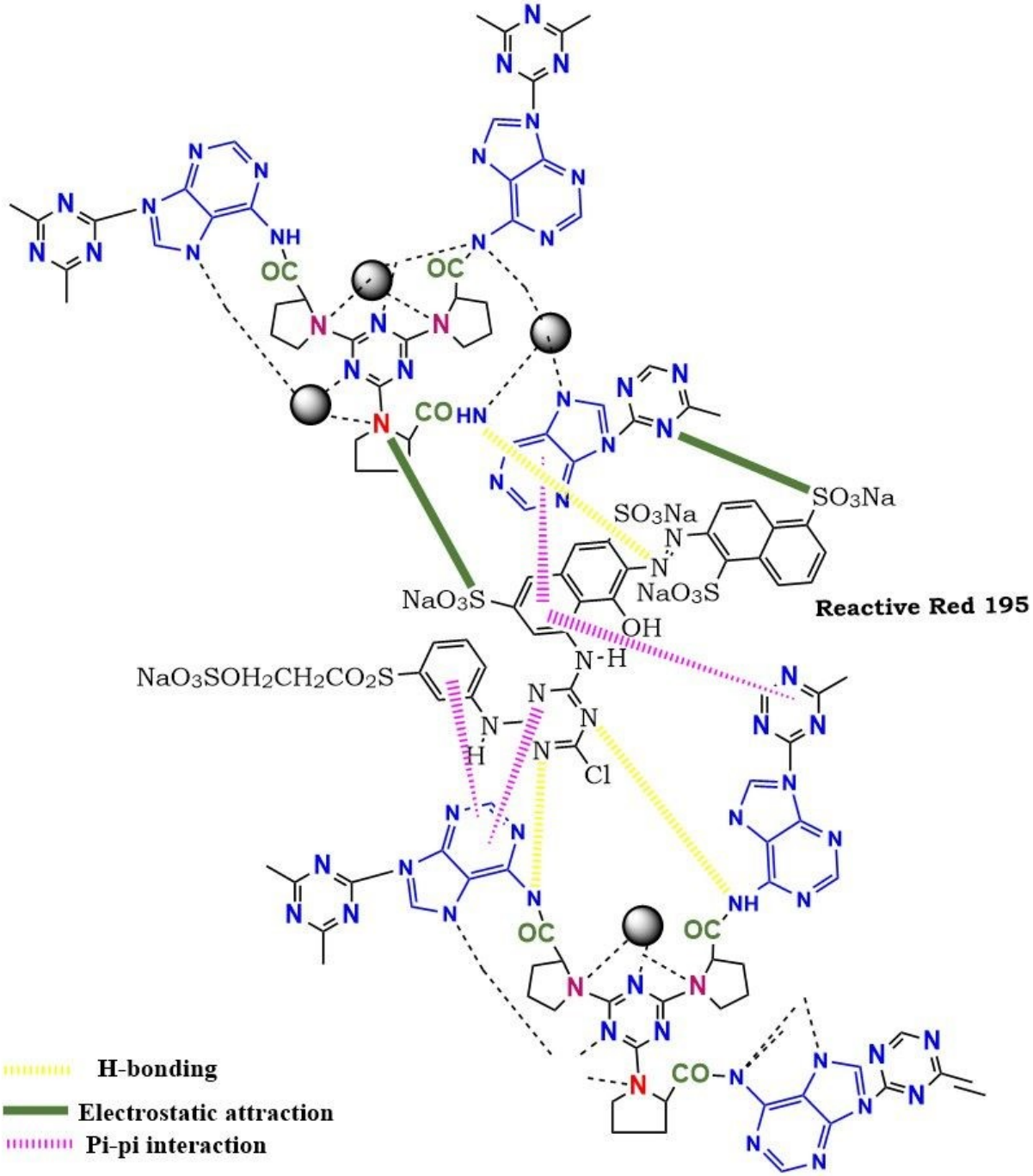

Fig. 17. Plausible interaction between Fe_3O_4-adn-(1,3,5-triazine-2,4,6-triyl)triproline nanocomposite and RR-195 dye molecule

View Article Online
DOI: 10.1039/D6MA00006A

Following dye adsorption, notable shifts and changes in the intensity of characteristic bands corresponding to Fe-O bonds (~580 cm^{-1}), triazine C=N vibrations (1500-1650 cm^{-1}), and -OH/-NH stretching (3200-3500 cm^{-1}) were noted. These spectral changes show that the surface functional groups are directly involved in the adsorption process. While changes in the triazine ring vibrations support π-π interactions between the adsorbent and aromatic dye molecules, the shift in -OH/-NH bands suggest hydrogen bonding interactions.

The main function of the Fe_3O_4 nano particles in the triazine-functionalised nanocomposite is to act as a magnetic core, which enables quick magnetic separation and simple adsorbent recovery treatment. Nonetheless, hydroxyl groups(-OH) are commonly found on the surface of Fe_3O_4 nano particles, and these groups may also take part in adsorption through weak coordination interaction or hydrogen bonding with dye molecules. However, the nitrogen-rich triazine functional groups provide the dominant adsorption sites and encourage strong interactions with reactive dyes through π-π interactions and electrostatic attraction. A multifunctional triazine modified magnetic polymeric network facilitate the effective adsorption reactive dyes via synergistic electrostatic, hydrogen bonding-bonding and π-π interactions, while included Fe_3O_4 nano particles provide quick magnetic separation and superior recyclability.

3.7.9 Comparative analysis of adsorbents

Direct comparison of adsorption efficiency among various adsorbents is frequently problematic due to large variations in experimental circumstances, including pH, temperature, beginning dye concentration, and contact duration across different investigations. Nonetheless, despite these discrepancies, a comparative evaluation of adsorption capacities documented in the literature can yield significant insights. Table 3 displays a comparison of the highest adsorption capabilities of several adsorbents documented for removal of RR-195 dye. The adsorption capabilities of the Fe_3O_4-adn-(1,3,5-triazine-2,4,6-triyl)triproline nanocomposite created in this study exhibits enhanced performance compared to several previously reported materials, affirming its high affinity and efficiency for the removal of dye from aqueous environments.

Table 3 Comparison of recently reported magnetic triazine-based adsorbents and related Fe_3O_4 nanocomposites for dye removal from aqueous solutions

Sr. No.	Adsorbent	Target Dye	Maximum adsorption Capacity (mg g^{-1})	Ref.
1.	CTF/Fe_2O_3	Methyl orange	219	40
2.	Magnetic covalent organic framework (Fe_3O_4 @TpPDA	Congo red	179.4	41
3.	Amino functionalised magnetic POP(FC-POP-EDA@ Fe_3O_4	Basic red	379.75	42
4.	Amino functionalised magnetic POP(FC-POP-EDA@ Fe_3O_4	Basic blue 41	240.9	42
5.	Fe_3O_4@tannic acid@ZIF-67	Cd(II)	215.5	43
6.	Fe_3O_4@tannic acid@ZIF-67	Mn(II)	138.9	43
7.	Phenolate-rich anionic covalent organic frameworks	Basic green 1	302.70	44
8.	Phenolate-rich anionic covalent organic frameworks	Methylene Blue	279.97	44
9.	Fe_3O_4-adn-(1,3,5-triazine-2,4,6-triyl)triproline nanocomposite	Reactive red 195	909.9	Present study

4 Conclusion

Here, we successfully prepared Fe_3O_4-adn-(1,3,5-triazine-2,4,6-triyl)triproline nanocomposite that works well as an adsorbent for getting rid of dyes in industrial water and can be recovered magnetically. Structural and surface characterisation indicated triazine moieties were well anchored with Fe_3O_4 core, creating a stable hybrid framework with nitrogen-containing active sites. The nanocomposite kept its super magnetic properties, which made it easy and quick to separate the magnetic particles once they have been absorbed. Adsorption test showed that industrial reactive dyes could be removed very well. This was due to a combination of electrostatic interaction, π-π stacking, hydrogen bonding, and surface complexation. Kinetic and isotherm investigations demonstrated a chemisorption-dominated on homogeneous surface, indicating monolayer adsorption characterised by dye-adsorbent interaction. The nanocomposite stood out for its great recyclability, as it kept a high adsorption capacity throughout many reuse cycles with almost no loss of performance. The fact that it is very efficient can be separated by magnets, and structurally stable shows that is might be used again and again. In general, the covalent triazine-capped Fe_3O_4 nanocomposite is a strong and long-lasting adsorbent for cleaning up dyes. The mechanistic insights and reusability exhibited in this study offer a valuable basis for the development of improved magnetic nanoparticles for effective wastewater treatment applications.

5 References

1. Oladimeji, T.E., Oyedemi, M., Emetere, M.E., Agboola, O., Adeoye, J.B. and Odunlami, O.A., Review on the impact of heavy metals from industrial wastewater effluent

and removal technologies. *Heliyon*, 2024, **10**(23), e40370, DOT:10.1016/j.heliyon.2024.e40370

2. Kayani, K. F., Bimetallic metal–organic frameworks (BMOFs) for dye removal: a review, *RSC advances*, 2024, **14**(43), 31777-31796, DOI:10.1039/D4RA06626J

3. Gökkuş, Ö., Brillas, E., and Sirés, I., Sequential use of a continuous-flow electrocoagulation reactor and a (photo) electro-Fenton recirculation system for the treatment of Acid Brown 14 diazo dye, *Science of the Total Environment*, 2024, **912**, 169143, DOI: 10.1016/j.scitotenv.2023.169143

4. Gökkuş, Ö. and Oğuz, Investigation of color and COD removal by Fenton reagent from aqueous solutions containing acid and reactive dyestuffs, *Desalination and Water Treatment*, 2011, **26**(1-3), 160-164, DOI: 10.5004/dwt.2011.2119

5. Nidheesh, P. V. and Gökkuş, Ö., Aerated iron electrocoagulation process as an emerging treatment method for natural water and wastewater, *Separation Science and Technology*, 2023, **58**(11), 2041-2063, DOI: 10.1080/01496395.2023.2227913.

6. Uddin, F., Environmental hazard in textile dyeing wastewater from local textile industry, *Cellulose*, **28**(17), 2021, 10715-10739, DOI: 10.1007/s10570-021-04228-4.

7. Lellis, B., Fávaro-Polonio, C. Z., Pamphile, J. A., and Polonio, J. C., Effects of textile dyes on health and the environment and bioremediation potential of living organisms, *Biotechnology Research and Innovation*, 2019, **3**(2), 275-290, DOI: 10.1016/j.biori.2019.09.001.

8. Ghosh, B., Saha, R., Bhattacharya, D., and Mukhopadhyay, M., Laccase and its source of sustainability in an enzymatic biofuel cell, *Bioresource Technology Reports*, 2019, **6**, 268-278, DOI: 10.1016/j.biteb.2019.03.013.

9. Hemashenpagam, N., and Selvajeyanthi, S., Textile dyes and their effect on human beings, In *Nanohybrid materials for treatment of textiles dyes*, Singapore: Springer Nature Singapore, 2023, 41-60, DOI: 10.1007/978-981-99-3901-5_3.

10. Mani, P., Fidal, V. T., Keshavarz, T., Chandra, T. S., and Kyazze, G., Laccase immobilization strategies for application as a cathode catalyst in microbial fuel cells for azo dye decolourization, *Frontiers in microbiology*, 2021, **11**, 620075, DOI: 10.3389/fmicb.2020.620075.

11. Ben Younes, S., Cherif, I., Dhouib, A., and Sayadi, S., Trametes trogii: A biologic powerful tool for dyes decolorization and detoxification, *Catalysis Letters*, 2016, **146**(1), 204-211, DOI: 10.1007/s10562-015-1629-x.

12. Zouari-Mechichi, H., Mechichi, T., Dhouib, A., Sayadi, S., Martínez, A. T., and Martinez, M. J., Laccase purification and characterization from Trametes trogii isolated in Tunisia: decolorization of textile dyes by the purified enzyme, *Enzyme and Microbial Technology*, 2006, **39**(1), 141-148, DOI: 10.1016/j.enzmictec.2005.11.027.

13. Chadha, U., Selvaraj, S. K., Thanu, S. V., Cholapadath, V., Abraham, A. M., Manoharan, M., and Paramsivam, V., A review of the function of using carbon nanomaterials in membrane filtration for contaminant removal from wastewater, *Materials Research Express*, 2022, **9**(1), 012003, DOI:10.1088/2053-1591/ac48b8.

14. Patel, S. R., Patel, I. R., Patel, N. H., and Patel, B. V., Microwave-assisted fabrication for synthesis of magnetite chitosan-modified polymer composite hydrogel as rapid removal adsorbent for effective remediation of hazardous contaminants, *Polymer Bulletin*, 2024, **81**(1), 449-473, DOI: 10.1007/s00289-023-04721-9.

15. Li, Y., An, Y., Zhao, R., Zhong, Y., Long, S., Yang, J., ... and Zheng, H., Synergetic removal of oppositely charged dyes by co-precipitation and amphoteric self-floating capturer: Mechanism investigation by molecular simulation. *Chemosphere*, 2022, **296**, 134033, DOI:10.1016/j.chemosphere.2022.134033.

16. Bharucha, S. R., Dave, M. S., Chaki, S. H., and Limbani, T. A., Thermal investigation of NbSe 2 nanoparticles synthesized through a temperature-dependent sonochemical method, *RSC advances*, 2024, **14**(45), 33459-33470, DOI:10.1039/D4RA05108D.

17. Pan, D., Song, Y., Liu, C., and Guo, Z., Research progress on wastewater treatment in food industry: a mini-review, *ES Food & Agroforestry*, 2022, **10**(2), 10-23, DOI: 10.30919/esfaf793.

18. Soni, S., Bajpai, P. K., Mittal, J., and Arora, C., Utilisation of cobalt doped Iron based MOF for enhanced removal and recovery of methylene blue dye from waste water, *Journal of Molecular Liquids*, 2020, **314**, 113642, DOI: 10.1016/j.molliq.2020.113642.

19. Afkhami, A., and Moosavi, R., Adsorptive removal of Congo red, a carcinogenic textile dye, from aqueous solutions by maghemite nanoparticles, *Journal of hazardous materials*, 2010, **174**(1-3), 398-403, DOI: 10.1016/j.jhazmat.2009.09.066.

20. Qadri, S., Ganoe, A., and Haik, Y., Removal and recovery of acridine orange from solutions by use of magnetic nanoparticles. *Journal of hazardous materials*, 2009, *169*(1-3), 318-323. DOI:10.1016/j.jhazmat.2009.03.103

21. Zhou, L., Gao, C., and Xu, W., Magnetic dendritic materials for highly efficient adsorption of dyes and drugs. *ACS applied materials & interfaces*,2010, *2*(5), 1483-1491. DOI: 10.1021/am100114f.

22. Mak, S. Y., and Chen, D. H., Fast adsorption of methylene blue on polyacrylic acid-bound iron oxide magnetic nanoparticles, *Dyes and pigments*, 2004, **61**(1), 93-98, DOI: 10.1016/j.dyepig.2003.10.008.

23. Wang, D. W., Li, F., Lu, G. Q., and Cheng, H. M., Synthesis and dye separation performance of ferromagnetic hierarchical porous carbon, *Carbon*, 2008, **46**(12), 1593-1599, DOI: 10.1016/j.carbon.2008.06.052.

24. Yang, N., Zhu, S., Zhang, D., and Xu, S., Synthesis and properties of magnetic Fe3O4-activated carbon nanocomposite particles for dye removal. *Materials Letters*, 2008, **62**(4-5), 645-647, DOI: 10.1016/j.matlet.2007.06.049.

25. Oliveira, L. C., Rios, R. V., Fabris, J. D., Garg, V., Sapag, K., and Lago, R. M., Activated carbon/iron oxide magnetic composites for the adsorption of contaminants in water, *Carbon*, 2002, **40**(12), 2177-2183, DOI:10.1016/S0008-6223(02)00076-3.

26. Ai, L., Huang, H., Chen, Z., Wei, X., and Jiang, J., Activated carbon/CoFe2O4 composites: facile synthesis, magnetic performance and their potential application for the removal of malachite green from water, *Chemical Engineering Journal*, 2010, **156**(2), 243-249, DOI: 10.1016/j.cej.2009.08.028.

27. Ejaz, M., Mohamed, M. G., Kotp, M. G., Elewa, A. M., and Kuo, S. W., Triphenylamine-linked triazine (DA) units based hypercrosslinked porous polymer: Rapid adsorption and enhanced photodegradation of organic dyes from water, *Colloids and Surfaces A: Physicochemical and Engineering Aspects*, 2025, 137239, DOI: 10.1016/j.colsurfa.2025.137239.

28. Shafqat, S. S., Sumrra, S. H., Zafar, M. N., Aslam, S., Vohra, M. I., Nosheen, M., ... and Khan, M. A., Modification of amino functionalized silica nanoparticles with L-proline and

furanacrylic acid as novel composites for the efficient removal of methyl orange, *Materials Today Communications*, 2024, **39**, 108934, DOI: 10.1016/j.mtcomm.2024.108934.

29. Ahmad, I., Abbasi, A., El Bahy, Z. M., and Ikram, S., Synergistic effect of silver NPs immobilized on Fe3O4@ L-proline magnetic nanocomposite toward the photocatalytic degradation of Victoria blue and reduction of organic pollutants, *Environmental Science and Pollution Research*, 2023, **30**(32), 78891-78912, DOI:10.1007/s11356-023-27837-x.

30. Maleki, A., and Firouzi-Haji, R., L-Proline functionalized magnetic nanoparticles: A novel magnetically reusable nanocatalyst for one-pot synthesis of 2, 4, 6-triarylpyridines, *Scientific reports*, 2018, **8**(1), 17303, DOI:10.1038/s41598-018-35676-x.

31. Wu, J., Liu, J., Wen, B., Li, Y., Zhou, B., Wang, Z., ... and Zhao, R., Nitrogen-rich covalent triazine frameworks for high-efficient removal of anion dyes and the synergistic adsorption of cationic dyes, *Chemosphere*, 2021, **272**, 129622, DOI:10.1016/j.chemosphere.2021.129622

32. Ahmadijokani, F., Ahmadipouya, S., Haris, M. H., Rezakazemi, M., Bokhari, A., Molavi, H., ... and Arjmand, M., Magnetic nitrogen-rich UiO-66 metal–organic framework: an efficient adsorbent for water treatment, *ACS Applied Materials & Interfaces*, 2023, **15**(25), 30106-30116, DOI:10.1021/acsami.3c02171

33. Peter, S. E., Bera, A., Vennapusa, S. R., Vairavel, P., and Kumar, N. V. A., From Computational Screening to Enhanced Adsorption: Optimized Removal of Toxic Congo Red by Nitrogen-rich Triazine Polymers, *Macromolecular Materials and Engineering*,2025, e00366, DOI:10.1002/mame.202500366

34. Divya, Kalla, S., and Jangir, R., Azo-linked nanoporous organic polymer for efficient capture of cationic dyes and radioactive iodine, *Journal of Materials Science*, 2025, 1-22, DOI:10.1007/s10853-025-11816-3

35. Abolghasemi, S., Nasiri, A., Hashemi, M., Rajabi, S., and Rahimi, F., Magnetic nanocomposites: innovative adsorbents for antibiotics removal from aqueous environments–a narrative review, *Applied Water Science*, 2025, **15**(2), 30, DOI:10.1007/s13201-025-02360-1

36. Mehmood, A., Khan, F. S. A., Mubarak, N. M., Tan, Y. H., Karri, R. R., Khalid, M., ... and Mazari, S. A., Magnetic nanocomposites for sustainable water purification—a comprehensive review, *Environmental Science and Pollution Research*, 2021, **28**(16), 19563-19588, DOI:10.1007/s11356-021-12589-3

37. Rocha, L. S., Sousa, É. M., Pereira, D., Gil, M. V., Otero-Irurueta, G., Gallo, M. J. H., ... and Calisto, V., Sustainable and recoverable waste-based magnetic nanocomposites used for the removal of pharmaceuticals from wastewater, *Chemical Engineering Journal*, 2021, **426**, 129974, DOI:10.1016/j.cej.2021.129974

38. Yadav, D., and Awasthi, S. K., Recent advances in the design, synthesis and catalytic applications of triazine-based covalent organic polymers, *Materials Chemistry Frontiers*, 2022, **6**(12), 1574-1605, DOI:10.1039/D2QM00071G

39. Peralta, M. E., Ocampo, S., Funes, I. G., Onaga Medina, F., Parolo, M. E., and Carlos, L., Nanomaterials with tailored magnetic properties as adsorbents of organic pollutants from wastewaters, *Inorganics*, 2020, **8**(4), 24, DOI:10.3390/inorganics8040024

40. Zhang, W., Liang, F., Li, C., Qiu, L. G., Yuan, Y. P., Peng, F. M., ... and Zhu, J. F., Microwave-enhanced synthesis of magnetic porous covalent triazine-based framework composites for fast separation of organic dye from aqueous solution, *Journal of Hazardous materials*, 2011, **186**(2-3), 984-990, DOI:10.1016/j.jhazmat.2010.11.093

41. Lu, S., Wei, Y., Long, S., Chen, Z., Chen, F., Lin, H., and Lu, J., Efficient adsorption and removal of congo red from aqueous solution using magnetic covalent organic framework nanocomposites, *ChemistrySelect*, 2023, **8**(1), e202203621, DOI:10.1002/slct.202203621

42. Taheri, N., and Dinari, M., Amino-functionalized magnetic porous organic polymer for the selective removal of toxic cationic dyes from textile wastewater, *New Journal of Chemistry*, 2022, **46**(23), 11174-11184, DOI:10.1039/D2NJ01754G

43. Wu, J., Xiang, Z., Li, Y., Lv, J., and Peng, X., PSS-Functionalized Fe3O4/ZIF-67 Nanocomposite: An Efficient Adsorbent for Rapid Removal of Microplastics From Wastewater, *ChemistrySelect*, 2026, **11**(6), e06885, DOI:10.1002/slct.202506885

44. Nozaki, M., Irie, T., Sasaki, K., Sasikumar, S., Kawawaki, T., Maricherla, H., and Negishi, Y., Phenolate-Rich Anionic Covalent Organic Frameworks with Engineered Reticular Microenvironments Enable Selective Dye Capture from Model Solutions and Real Textile Wastewater, 2026, DOI:10.26434/chemrxiv.15000563/v1

View Article Online
DOI: 10.1039/D6MA00006A

Data Availability Statement for title: "Covalent triazine-capped Fe_3O_4 nano composite for efficient dye remediation: structural insights, adsorption mechanism, and recyclability"

The datasets generated/analyzed during the current study are presented in the article.